PROCEEDINGS, 49th Workshop on Geothermal Reservoir Engineering
Stanford University, Stanford, California, February 12-14, 2024
SGP-TR-227

Source Characterization of Picoseismic Events During Hydraulic Stimulation at Hectometer Scale

Martina Rosskopf, Virginie Durand, Linus Villiger, Anne Obermann, Domenico Giardini and the Bedretto Team

Institute of Geophysics, ETH Zurich, Sonneggstrasse 5, CH-8092 Zurich

martina.rosskopf@erdw.ethz.ch

Keywords: Induced seismicity, source characterization, hydraulic stimulation, EGS, BedrettoLab, hectometer scale

ABSTRACT

From 2021 to 2023, we performed 17 hydraulic stimulations at hectometer scale in a fully controlled environment in the Bedretto tunnel. The Bedretto tunnel is a new research facility below the Swiss Alps with an overburden of 1 km. For the experiments, a multi-packer system was installed in a 400 m long stimulation borehole, dividing it into 14 intervals. Additionally, a densely spaced multi-component geophysical monitoring system was installed in six surrounding monitoring boreholes. Information on in-situ stress conditions were collected prior to the stimulations from all boreholes.

A first analysis of the data showed that the dense network allowed us to resolve the seismic event locations well beyond point clouds. The seismic event locations reveal clear alignments which reflect the activation of the faults in the rock volume in space and time. In addition to the highly resolved event locations, we are able to estimate well constrained moment tensors for the picoseismic events. The moment tensors align with the known fractures and reveal differences in the mechanism between faults within short distances (<10 m).

1. INTRODUCTION

In the future, geothermal energy is expected to play an important role in the energy production using the constant high heat conditions in the deep underground. Currently, geothermal fields are primarily confined to regions with favorable geological conditions, such as naturally fractured hydrothermal systems (Majer et al., 2007; Gischig et al., 2020). Other regions exist where the subsurface heat is sufficient, but the permeability of the targeted rock volume is insufficient for heat and energy extraction. Enhanced Geothermal Systems (EGS) offer a solution to overcome these challenging conditions. Through hydraulic stimulations, EGS can increase the permeability in crystalline basement rock (Evans et al., 2005). The increased permeability enables the fluid circulation between an injection and a production borehole, creating a heat exchanger (Majer et al., 2007). The key challenge for EGS reservoirs is the need to increase the permeability to create and maintain flow pathways in high temperature rock volumes, but at the same time keeping the induced seismicity at a low level (Kwiatek et al. 2019; Ellsworth et al., 2019). Past EGS projects, such as Basel (Deichmann and Giardini, 2009; Kraft et al., 2009) and Pohang (Ellsworth et al., 2019), needed to be terminated because the induced seismicity was widely felt and damaged infrastructure. Therefore, to unlock the full potential of EGS a deeper understanding of the connection between seismicity and thermo-hydromechanical properties during hydraulic stimulations is needed (Gischig et al., 2020).

Most studies on the interplay of seismicity and fluid injections are either from experiments on the laboratory scale or on the field scale, which differ by at least three orders of magnitude (Gischig et al., 2020). To close this gap, experiments on the intermediate scale are needed. These in-situ injection experiments on the intermediate scale hold the advantage of good sensor coverage and sufficient access to the reservoir comparable to the laboratory scale. Additionally, they replicate similar complex rock conditions as those found on the field scale. Therefore, the rock volume and the processes during hydraulic stimulations can be studied in great detail. Such an underground laboratory for injection experiments on the intermediate scale was developed by ETH Zurich in the Bedretto Tunnel in the Swiss Alps.

2. TEST SITE AND HYDRAULIC STIMULATION

The Bedretto Underground Laboratory for Geoenergies and Geosciences (BULGG or BedrettoLab) is a new research facility operated by ETH Zurich. It is located in the 5.2 km long Bedretto Tunnel in the southern Swiss Alp in Ticino, connecting the Furka Base Tunnel in the northwest with the Bedretto valley in the southeast (Rast et al., 2022). The Bedretto geothermal TestBed is at 2 km of the tunnel with an overburden of 1000 m and an approximate dimension of 100 m x 300 m x 100 m. The rock around the TestBed is relatively homogeneous granite, the Rontondo granite (Keller and Schneider, 1982). The stress regime is controlled by normal and/or strike-slip faulting (Ma et al., 2022; Bröker and Ma, 2022). Most structures are NE-SW to E-W striking with a steep dip above 50° (Bröker et al., 2024). Ma et al. (2022) characterized the rock volume by three separated units, a middle fault zone and two sandwiching units above and below the fault zone.

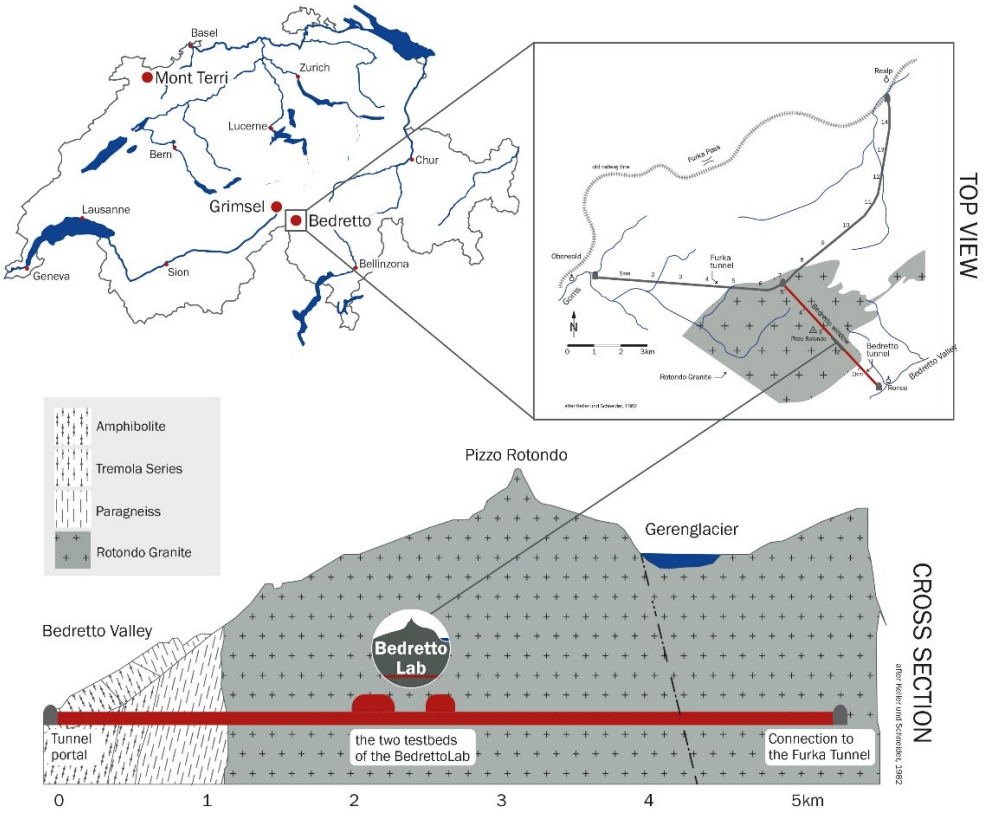

Figure 1: Overview of the Bedretto Tunnel in Ticino, its geological setting and the location of the Geothermal TestBed in the Tunnel marked to the left of the BedrettoLab sign (modified after Rast et al., 2022, BedrettoLab at ETH Zurich)

Within the target rock volume, 7 monitoring boreholes (MB) and 2 stimulation/production boreholes (ST) with 100 m-400 m length were drilled. The ST1 borehole, where the injections took place, is equipped with a multipacker system dividing the borehole into 14 intervals. By dividing the borehole into smaller intervals, smaller sections of the rock volume can be targeted by the fluid injections. In the surrounding monitoring boreholes, a multi-component geophysical monitoring system was installed, including pressure, strain, temperature, and seismic sensors (Plenkers et al.,2023). The seismic sensors consist of borehole geophones, accelerometers, and acoustic emission sensors to cover a wide range of frequencies (0.08 Hz-50 kHz). This setup holds the opportunity to record seismic events down to M-5. More detailed information on the monitoring system can be found in Plenkers et al. (2023).

In 2021 to 2023, 17 injection experiments were performed in the intervals 7 to 14 (top interval). These intervals are located within the densest part of the multi-component monitoring system. The stimulations can be grouped into two phases. The goal of phase 1 was to characterize the hydro-mechanical properties of each interval, using similar injection protocols, consisting of 2 pressure-controlled and 6 fluid rate-controlled injection cycles that were stopped when the jacking pressure was reached. Since the jacking pressure depends on the geological setting of each interval, different total volumes of water (0.3 to 14.1 m^3) were injected. In phase 2, specific intervals (interval 8, 9, 10, 11, 12) that showed interesting behavior in seismicity, transmissivity, or pressure evolution in phase 1, were stimulated again. Here, the goal was to see how the rock volume behaves in terms of reservoir engineering for longer injection durations. Therefore, much higher fluid volumes (2.4 to 273.8 m^3) were injected, continuing beyond the jacking pressure. More information on the stimulation protocols can be found in Obermann et al. (2024) and Bröker et al. (2024).

3. SEISMIC DATA PROCESSING

The continuous seismic data of the installed acoustic emission sensors (AE sensors) and accelerometers are acquired with DUGseis, a python-based software specifically developed for high-frequency (MHz) acoustic emission recordings. Waveform data is recorded and stored in the ASDF format (Greenfield et al., 2015; D'Avella et al., 2023) using specific Spectrum digitizer cards. The data streams are then directly transferred to a server in Zurich. From there, we are able to access the data in quasi real-time (i.e. with ~10 s delay) or in a post-processing mode with the DUGseis software for data processing (Rosskopf et al. 2024).

3.1 Extracting a Seismic Catalog

Several steps are necessary to extract a high-quality seismic catalog from the raw waveform data (waveform examples of one event are shown in Figure 2). For the stimulations in the BedrettoLab, we distinguish between procedures for real-time, advanced real-time and post-processing. The first step of all procedures is the application of a standard STA/LTA picker and associater on the 5 sensors closest

to the injection point to obtain a list of potential event candidates. In the real-time procedure, we apply an additional STA/LTA picker algorithm on all sensor traces of our network within a time window of 40 ms around an event candidate's onset. If an event candidate has at least 8 picks, it is located and a magnitude is estimated. For all procedures, we use a simple location algorithm, where event locations are estimated by fitting the P-arrival times to a homogenous velocity model.

The purpose of the advanced real-time procedure is to improve the pick and location accuracy of the somewhat imprecise STA/LTA results, especially for small events. We apply a multi-frequency band kurtosis picker (FBKT) (Poiata et al. (2016)) on the 20 closest sensors. This picker is slower than the STA/LTA picker and, therefore, is run in parallel to the first real-time procedure. The resulting refined picks give a better image of the spatio-temporal evolution during stimulation. As the name suggests, the post-processing procedure is applied after a stimulation is completed. Here, the FBKT picker is applied on all available channels. For small events, the FBKT picker often picked the minimum or maximum amplitude after the onset. Therefore, as an additional refinement of the onset picking, we apply another picking algorithm, the autoregressive-Akaike information criteria picker (Maeda, 1985; Leonard and Kennett, 1999; Bagagli, 2021a). Again, the same location algorithm is used as in real-time, but in addition, we also apply a relative relocation using the double difference event relocation method by Waldhauser and Ellsworth (2000).

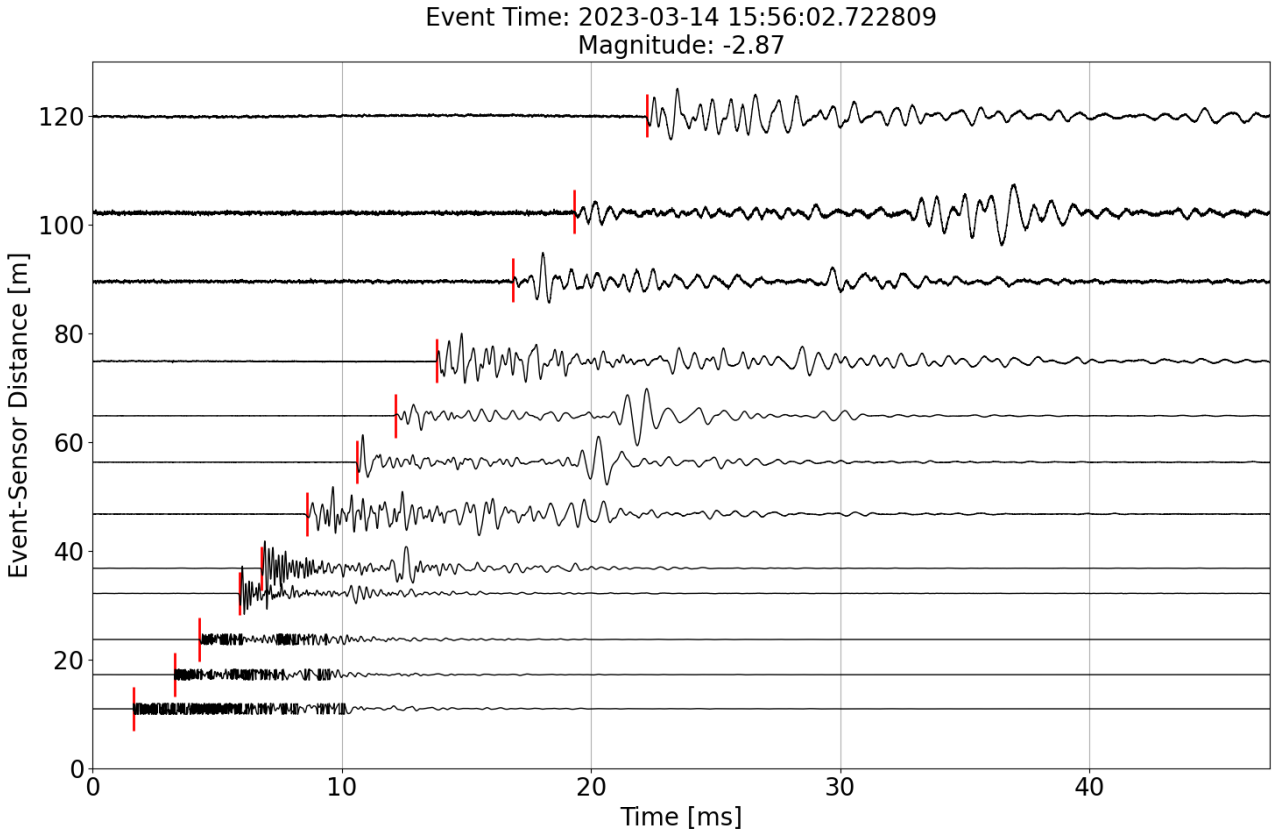

Figure 2: Waveforms of a Mw -2.87 event in interval 9 phase 2. The event is visible to a distance of 120 m with clear P- and S-wave onsets. The different waveform traces were normalized by their maximum amplitudes. The closest sensors to the event show clipped waveforms.

3.2 Moment Tensor Inversion

Only few studies (e.g. Zang et al., 2017; Kwiatek et al., 2011, Kwiatek et al., 2018; Villiger et al., 2021) perform source analyses for micro- and picoseismic events due to the typically limited azimuthal coverage of such small events. Here, we are in the exceptional situation of an advantageous spherical coverage and short source-receiver distances for a large number of events. This comprehensive dataset enhances our ability to analyze and understand the complex seismic processes occurring in the subsurface.

To study source mechanisms of the seismic events, we performed moment tensor inversion using the HybridMT software package (Kwiatek et al., 2016). The software uses the P-wave onset amplitude and its polarity to estimate double constrained (DC), deviatoric and full moment tensors (FMT). HybridMT includes an iterative procedure to account for poorly known pathway, site and sensors effects (Andersen, 2001). Therefore, it was necessary to spatially cluster the events first. Within one cluster, similar ray paths can be assumed if the events have small inter-event distances compared to the event-sensor distances. We distinguished clusters by using the clustering method HDBSCAN from the scikit-learn package (Pedregosa et al. 2011). We applied the clustering method on events with minimum 12 P-onsets and Signal-to-Noise Ratio (SNR) greater 10, which were detected during stimulations in phase 1 and 2A in the central interval

12. Events within 1 m distance to each other were considered in one cluster. The clustering was done separately for each phase. The moment tensor inversion was performed for each cluster individually. Information needed for the inversion, such as sensor locations, takeoff angle, omega (the area below the first P-wave pulse) and polarity were given to hybridMT. The software processed and resolved these inputs to moment tensors (MT). To evaluate uncertainties, we estimated each MT 100 times with a resampled input datasets, which means besides the original given dataset, hybridMT generates 100 times "new" input datasets assuming 5% wrongly picked polarities and adds a random bias on the takeoff angle of approximately 3 degrees. With this resampling of data, HybridMT computed 100 possible solutions for the MT which we evaluated by estimating the Kagan angles, the angle between the different fault solutions. Moment tensors with Kagan angles above 20 degrees were discarded for further analysis because no clear moment tensor solution could be chosen.

4. RESULTS

In the following section, we highlight some features from the spatial distribution of the seismicity during the stimulations and give first insights into the source mechanisms of two interval 12 stimulations.

4.1 Spatial Distribution of Seismic Clouds during Stimulation

In Figure 3, we display the overall seismicity of 14 of the 17 stimulations in 8 different intervals (Obermann et al., 2024). Here, we only show high quality events and remove scattered events, which means the events were detected on at least 8 sensors and have more than 40 neighboring events. The seismicity in Figure 3 aligns in multiple elongated streaks, striking in NE-SW direction with a dip of around 70-80 degree. This strike and dip direction is in agreement with pre-existing faults known from previous studies (Ma et al., 2022; Bröker et al., 2024).

In phase 1, despite the similarity in the injection protocols, the seismic event rate and spatial extent of the seismic cloud varied greatly. For instance, the phase 1 stimulation in interval 11 resulted in a rather small number of only 99 events, whereas in interval 13 more than 5000 events were detected. The spatial extension of the seismic clouds varied between 7 m (interval 12) and 90 m (interval 7).

During the phase 2 stimulations, the intervals were stimulated much longer, with higher injection volumes. As expected, this resulted in a much higher total event number and the lateral extent of the seismicity cloud was larger compared to the first phase. This means seismicity in the second phase shows fault reactivation over longer areas of different fault structures. Additionally, the seismicity shows that fractures were reactivated which have not been reactivated in the first phase.

In Figure 3 the events of interval 8, interval 9+10 (jointly stimulated in phase 2), interval 11 and interval 13 dominate, since their number of events (between ~2400 and ~12700) and spatial extent (between 40 m to 130 m) are the highest. With ongoing stimulation in intervals 8, 9+10 and 11, the seismicity is moving upwards towards the tunnel, reaching other fractures of the intervals above.

Seismicity of interval 12 showed the smallest spatial extent (7 m in phase 1, 15 m in phase 2A and 8 m in phase 2B) and only small amounts of water were injected (between 0.3 and 2.9 m^3 per phase). Nevertheless, the pressure in interval 12 during stimulation was the highest in comparison to all other stimulations. The number of recorded events of 241, 500 and 683 for phase 1, 2A and 2B, respectively, was rather small compared to other intervals. In phase 1 two structures with NE-SW direction were stimulated, one located at the bottom and the other located in the middle of the interval. In phase 2A and 2B (re-stimulated twice in phase 2) the same structures were reactivated additionally to a third structure, located at the top part of the interval. The third structure was reactivated suddenly during the second cycle of the phase 2A stimulation and only a small number of the events were located there. In phase 2B, the main stimulated structures with most seismicity were the middle and the top structure.

Overall, the seismicity in each interval varies significantly in terms of number of events and spatial extent. For most intervals, multiple fractures were stimulated, as visible in Figure 3. Only during the interval 13 stimulation a single fault structure was stimulated. This fault structure is the most dominant shear zone in the Geothermal TestBed. The event locations of all stimulations nicely follow structures within the rock volume, which highlight the faults reactivated due to the hydraulic injections. The maximum magnitude of Mw -1.64 was detected during the interval 8 stimulation. This is also the stimulation which activated the largest volume. Overall, we were able to detect events with magnitudes as low as Mw -5. The magnitude of completeness lies around Mw -4.3.

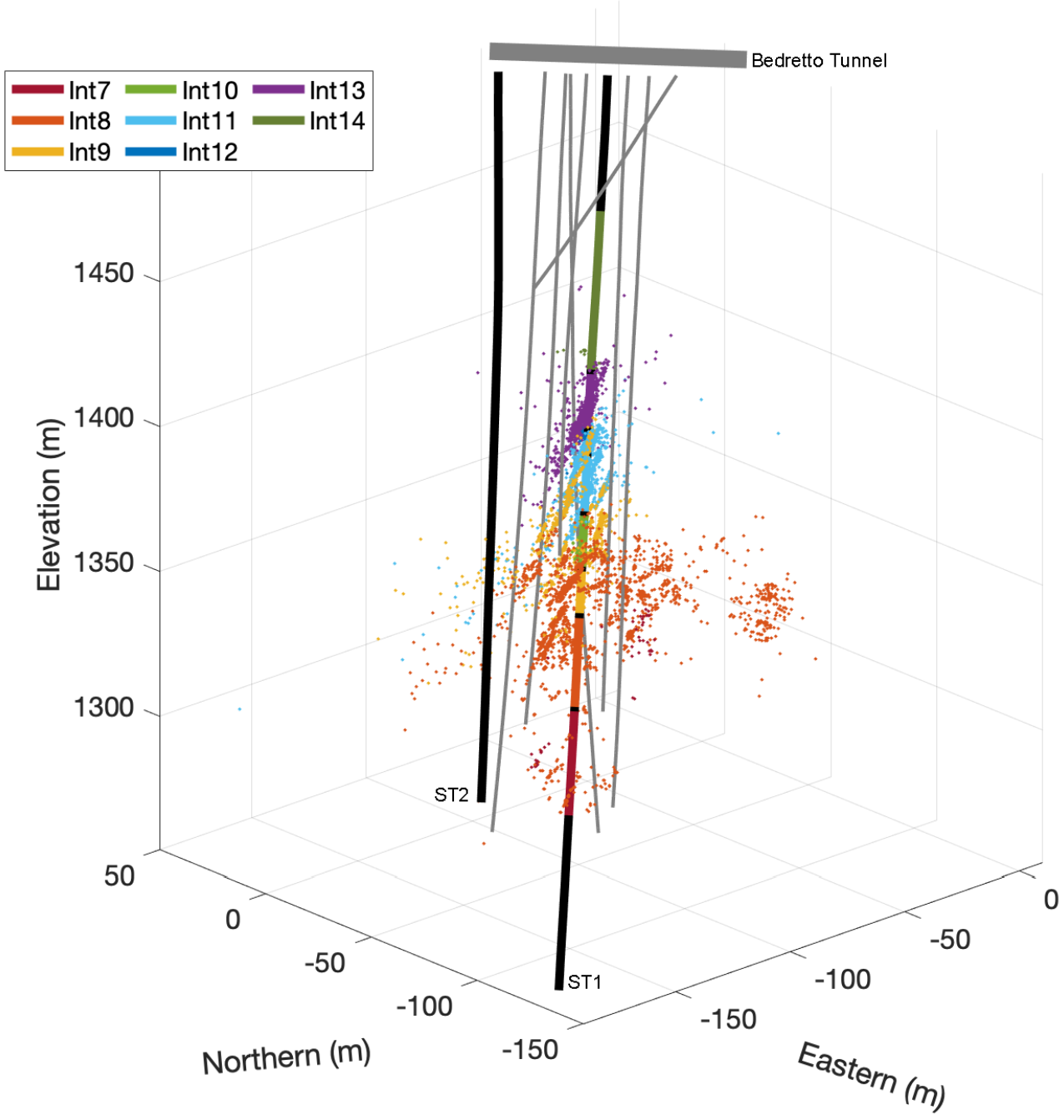

Figure 3: Seismic events recorded during the hydraulic stimulation experiments. The colors represent the seismicity in the different intervals. The dark black lines display the stimulation boreholes, ST1 as the injection borehole and ST2 as the production borehole. The colors on the ST1 borehole indicate the locations of the different intervals. The gray lines are the monitoring boreholes (Figure modified after Obermann et al., 2024).

4.2 Source Mechanisms of Seismicity

In this subsection, we present first results of moment tensors estimated for the interval 12 stimulations in phase 1 and phase 2A (Fig. 4). As stated in the previous section, 2 spatially separated clusters were reactivated during phase 1, whereas in phase 2A an additional third structure was reactivated. In Figure 4, the different clusters are shown, where the third structure is represented by cluster 3 in Figure 4B. The clusters 1 and 2 show the two fault structures that were activated during both injection phases 1 and 2A. Moment tensors were estimated for all clusters. Figure 4 displays the most dominant moment tensor of cluster 1 in phase 1 (Fig. 4A) and cluster 2 in phase 2 (Fig. 4B). For cluster 1 during phase 1 and cluster 2 during phase 2, we were able to resolve moment tensors for 48 of 55 and 60 of 78 events, respectively. The moment tensors of the other events were discarded because they showed Kagan angles above 20 degrees and, therefore, high uncertainties in the solutions. The projection of the beach balls in Figure 4 is adjusted to the view of the event locations.

The colored lines of the beach balls represent the selected fault plane. The mechanism of phase 1, cluster 1 is dominated by strike-slip faulting and for phase 2, cluster 2 normal faulting is the dominant mechanism. The computed focal mechanisms nicely align with the seismicity which follows the fault structures.

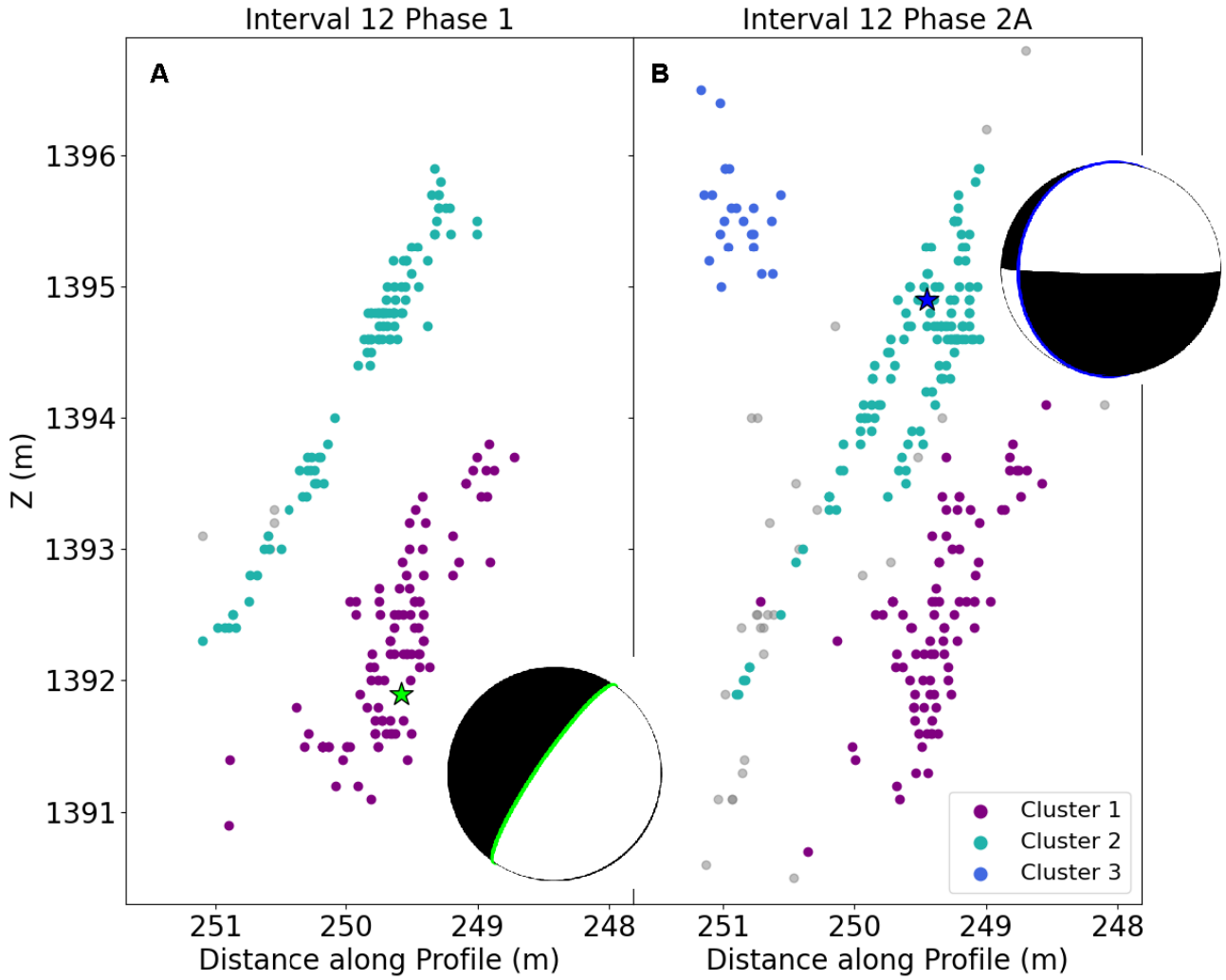

Figure 4: Seismicity clusters of interval 12 stimulations in phase 1 (A) and phase 2A (B). The beach balls represent the source mechanism of the events marked with stars. They show the most dominant source mechanism of the respective cluster.

5. CONCLUSION

The seismicity occurring during the hydraulic stimulations is a clear indicator for the flow path of the injected water. With our experiments and the monitoring system in place, we are able to resolve seismic event locations beyond point clouds and map them together with the fault structures on the hectometer scale. Here, we see clear alignments with preexisting faults in the different intervals. The various behaviors of the different intervals (number of events, lateral extension, number of reactivated structures, magnitude) show the complexity of a fractured reservoir. Therefore, the geometry and fault structures within an interval seem to have an important influence on the rock response to fluid injection.

With the extended spherical coverage, we are able to compute large numbers of moment tensors. The first results of interval 12 highlight that focal mechanisms can change between closely located fractures (<10m). The two dominant focal mechanisms of strike-slip (cluster 1) and normal faulting (cluster 2) are in agreement with a previous study done by Bröker and Ma (2022) who showed that the rock volume is dominated by normal and strike-slip faulting. In the future, we will extend the moment tensor analysis to see if changes of mechanism are visible within one cluster between phases. Additionally, the moment tensor inversion will be performed for other stimulations together with stress inversion from the resolved focal mechanisms, as done by Kwiatek et al. (2018). The stress inversions will allow us to learn more about the temporal evolution of the stress field during the performed stimulations. Combining our seismic results with the hydromechanical observations studied by Bröker et al. (2024) and Doonechaly et al. (2023), we will be able to understand the processes during stimulations in greater detail.

REFERENCES

Andersen, L., 2001. A Relative Moment Tensor Inversion Technique Applied to Seismicity Induced by Mining, University of the Witwatersrand.

Bagagli, M. (2021). Aurempickers. Zenodo. doi: 10.5281/zenodo.5459631.

Bröker, K., & Ma, X. (2022). Estimating the least principal stress in a granitic rock mass: systematic mini-frac tests and elaborated pressure transient analysis. Rock Mechanics and Rock Engineering, 55(4), 1931-1954. https://doi.org/10.1007/s00603-021-02743-1

Bröker, K., Ma, X., Doonechaly, N. G., Obermann, A., Rosskopf, M., Rinaldi, A. P., Hertrich, M., Serbeto, F., Maurer, H., Wiemer, S., Giardini, D., Bedretto Lab Team (2024). Hydromechanical characterization of a fractured crystalline rock during multistage hydraulic stimulations at the BedrettoLab. Manuscript in preparation.

D'Avella, D., Graham, B., Jamieson, W., Droettboom, M., Slavich, E., Robitaille, T., Dencheva,N., Greenfield, P., Simon, B., MacDonald, K., Bray, E. M., Burnett, Z., Davies, J., Mumford, S., Markovtsev, V., Tollerud, E., Sipőcz, B., Bradley, L., Fabry, Ç., Kerzendorf, W. (2023). Asdf-format/asdf: 3.0.1. Zenodo. https://doi.org/10.5281/zenodo.10054611

Deichmann, N. and Giardini, D. (2009). Earthquakes Induced by the stimulation of an enhanced geothermal system below Basel (Switzerland). Seismological Research Letters, 80(5):784–798.

Doonechaly, N. G., Hertrich, M., Bröker, K., Repolles, V. C., Shakas, A., Ma, X., Rinaldi, A. P., Gischig, V., Zilis, E., Hochreutener, R., Maurer, H., Wiemer, S., Giardini, D., (2023). Validation of Technologies for Reservoir Engineering (VALTER) - Phase-I Stimulation, Technical Report.

Ellsworth, W. L., Giardini, D., Townend, J., Ge, S., & Shimamoto, T. (2019). Triggering of the Pohang, Korea, earthquake (Mw 5.5) by enhanced geothermal system stimulation. Seismological Research Letters, 90(5), 1844-1858.

Evans, K. F., Genter, A., and Sausse, J. (2005). Permeability creation and damage due to massive fluid injections into granite at 3.5 km at Soultz: 1. Borehole observations. Journal of Geophysical Research: Solid Earth, 110(B4).

Gischig, V. S., Giardini, D., Amann, F., Hertrich, M., Krietsch, H., Loew, S., Maurer, H., Villiger, L., Wiemer,S., Bethmann, F., Brixel, B., Doetsch, J., Doonechaly, N. G., Driesner, T., Dutler, N., Evans, K. F., Jalali,M., Jordan, D., Kittilä, A., Ma, X., Meier, P., Nejati, M., Obermann, A., Plenkers, K., Saar, M. O.,Shakas, A., and Valley, B. (2020). Hydraulic stimulation and fluid circulation experiments in underground laboratories: Stepping up the scale towards engineered geothermal systems. Geomechanics for Energy and the Environment, 24.

Greenfield, P., Droettboom, M., & Bray, E. (2015). ASDF: A new data format for astronomy. Astronomy and Computing, 12, 240–251. https://doi.org/https://doi.org/10.1016/j.ascom.2015.06.004

Keller, F. and Schneider, T. R. (1982). Geologie und Geotechnik. Schweizer Ingenieur und Architekt, 100(24):512.

Kraft, T., Mai, P. M., Wiemer, S., Deichmann, N., Ripperger, J., Kästli, P., Bachmann, C., Fäh, D., Wössner, J., and Giardini, D. (2009). Enhanced Geothermal Systems: Mitigating Risk in Urban Areas.

Kwiatek, G., Plenkers, K., Dresen, G., & JAGUARS Research Group. (2011). Source parameters of picoseismicity recorded at Mponeng deep gold mine, South Africa: Implications for scaling relations. Bulletin of the Seismological Society of America, 101(6), 2592-2608.

Kwiatek, G., Martínez-Garzón, P., and Bohnhoff, M. (2016). HybridMT: A MATLAB/Shell Environment package for seismic moment tensor inversion and refinement. Seismological Research Letters, 87(4):964–976.

Kwiatek, G., Martínez-Garzón, P., Plenkers, K., Leonhardt, M., Zang, A., von Specht, S., ... & Bohnhoff, M. (2018). Insights into complex subdecimeter fracturing processes occurring during a water injection experiment at depth in Äspö Hard Rock Laboratory, Sweden. Journal of Geophysical Research: Solid Earth, 123(8), 6616-6635.

Kwiatek, G., Saarno, T., Ader, T., Bluemle, F., Bohnhoff, M., Chendorain, M., ... & Wollin, C. (2019). Controlling fluid-induced seismicity during a 6.1-km-deep geothermal stimulation in Finland. Science Advances, 5(5), eaav7224.

Leonard, M., & Kennett, B. L. N. (1999). Multi-component autoregressive techniques for the analysis of seismograms. Physics of the Earth and Planetary Interiors, 113(1-4), 247-263.

Ma, X., Hertrich, M., Amann, F., Bröker, K., Doonechaly, N. G., Gischig, V., Hochreutener, R., Kästli, P., Krietsch, H., Marti, M., Nägeli, B., Nejati, M., Obermann, A., Plenkers, K., Rinaldi, A. P., Shakas, A., Villiger, L., Wenning, Q., Zappone, A., Bethmann, F., Castilla, R., Seberto, F., Meier, P., Driesner, T., Loew, S., Maurer, H., Saar, M. O., Wiemer, S., and Giardini, D. (2022). Multi-disciplinary characterizations of the BedrettoLab-A new underground geoscience research facility. Solid Earth, 13(2):301–322.

Maeda, N. (1985). "A Method for Reading and Checking Phase Times in Autoprocessing System of Seismic Wave Data". In: Zisin 38.3, pp. 365–379. doi:10.4294/zisin1948.38.3_36.

Majer, E. L., Baria, R., Stark, M., Oates, S., Bommer, J., Smith, B., and Asanuma, H. (2007). Induced seismicity associated with Enhanced Geothermal Systems. Geothermics, 36(3):185–222.

Obermann, A., Rosskopf, M., Durand, V., Plenkers, K., Bröker, K., Doonechaly, N. G., Gischig, V., Hertrich, M., Kästli, P., Ma, X., Maurer, H., Rinaldi, A. P., Villiger, L., Wiemer, S., Zappone, A., Giardini, D. (2024). Picoseismic response of hectometer-scale

fracture systems to stimulation with cm-scale resolution under the Swiss Alps, in the Bedretto Underground laboratory. Journal of Geophysical Research. Manuscript submitted for publication.

Pedregosa, F., Varoquaux, G. and Gramfort, A. and Michel, V., Thirion, B. and Grisel, O. and Blondel, M. and Prettenhofer, P., Weiss, R. and Dubourg, V. and Vanderplas, J. and Passos, A., Cournapeau, D. and Brucher, M. and Perrot, M. and Duchesnay, E. (2011). Scikit-learn: Machine learning in Python. Journal of Machine Learning Research, 12, 2825-2830.

Plenkers, K., Reinicke, A., Obermann, A., Gholizadeh Doonechaly, N., Krietsch, H., Fechner, T., ... & Wiemer, S. (2023) Multi-Disciplinary Monitoring Networks for Mesoscale Underground Experiments: Advances in the Bedretto Reservoir Project. Sensors, 23(6), 3315.

Poiata, N., Satriano, C., Vilotte, J. P., Bernard, P., & Obara, K. (2016). Multiband array detection and location of seismic sources recorded by dense seismic networks. Geophysical Journal International, 205(3), 1548-1573.

Rast, M., Galli, A., Ruh, J. B., Guillong, M., & Madonna, C. (2022). Geology along the Bedretto tunnel: kinematic and geochronological constraints on the evolution of the Gotthard Massif (Central Alps). Swiss Journal of Geosciences, 115(1), 8.

Rosskopf, M., Durand, V., Villiger, L., Doetsch, J., Obermann, A., Krischer, L. (2024). DUGseis: A Python package for real-time and post-processing of picoseismicity. Journal for Open Source Software. Manuscript submitted for publication.

Villiger, L., Gischig, V. S., Kwiatek, G., Krietsch, H., Doetsch, J., Jalali, M., Amann, F., Giardini, D., & Wiemer, S. (2021). Meter-scale stress heterogeneities and stress redistribution drive complex fracture slip and fracture growth during a hydraulic stimulation experiment. Geophysical Journal International. https://doi.org/10.1093/gji/ggab057.

Waldhauser, F., & Ellsworth, W. L. (2000). A double-difference earthquake location algorithm: Method and application to the northern Hayward fault, California. Bulletin of the seismological society of America, 90(6), 1353-1368.

Zang, A.; Stephansson, O.; Stenberg, L.; Plenkers, K.; Specht, S.; Milkereit, C.; Schill, E.; Kwiatek, G.; Dresen, G.; Zimmermann, G.; et al. (2017) Hydraulic Fracture Monitoring in Hard Rock at 410 m Depth with an Advanced Fluid-Injection Protocol and Extensive Sensor Array. Geophys. J. Int., 208, 790–813.